

Emergence of Spike Correlations in Periodically Forced Excitable Systems

José A. Reinoso,^{1,*} M.C. Torrent,^{1,†} and Cristina Masoller^{1,‡}

¹*Departament de Física, Universitat Politècnica de Catalunya,
Colom 11, ES-08222 Terrassa, Barcelona, Spain*

(Dated: September 7, 2016)

In sensory neurons the presence of noise can facilitate the detection of weak information-carrying signals, which are encoded and transmitted via correlated sequences of spikes. Here we investigate relative temporal order in spike sequences induced by a subthreshold periodic input, in the presence of white Gaussian noise. To simulate the spikes, we use the FitzHugh-Nagumo model, and to investigate the output sequence of inter-spike intervals (ISIs), we use the symbolic method of ordinal analysis. We find different types of relative temporal order, in the form of preferred ordinal patterns which depend on both, the strength of the noise and the period of the input signal. We also demonstrate a resonance-like behavior, as certain periods and noise levels enhance temporal ordering in the ISI sequence, maximizing the probability of the preferred patterns. Our findings could be relevant for understanding the mechanisms underlying temporal coding, by which single sensory neurons represent in spike sequences the information about weak periodic stimuli.

PACS numbers: 05.45.Tp; 87.19.lj; 89.70.Cf

INTRODUCTION

Many excitable systems, such as neurons and cardiac cells, display spiking output signals that can be analyzed by using an event-level approach, i.e., by detecting the times when the spikes occur, and then analyzing the statistics of the time intervals between successive spikes (inter-spike intervals, ISIs). Some important properties of ISI sequences are related to coherence and stochastic resonance phenomena. Coherence resonance refers to enhanced spike regularity under an optimal level of noise [1], while stochastic resonance refers to enhanced detection and transmission of subthreshold time-varying signals, also under an optimal level of noise [2–5].

Another relevant property of ISI sequences is the presence of correlations [6–9], which are known to influence the neuron’s capacity of information transfer [10–13]. In particular, while Gaussian white stochastic stimuli produce uncorrelated ISI sequences, correlated stochastic stimuli and information-carrying stimuli generate correlated spikes [14–17].

In the literature, temporal correlations in ISI sequences have been quantified by means of the serial correlation coefficients (SCCs), C_j ,

$$C_j = \frac{\langle (I_i - \langle I \rangle) (I_{i-j} - \langle I \rangle) \rangle}{\sigma^2}, \quad (1)$$

where j is an integer number, $\{\dots I_{i-1}, I_i, I_{i+1} \dots\}$ is the ISI sequence, and $\langle I \rangle$ and σ are the mean value and the standard deviation of the ISI distribution.

SCCs and statistical analysis of the ISI distribution are standard techniques to investigate spike trains. In the last decade, however, nonlinear methods of time-series analysis have been demonstrated useful for extracting information from empirical or synthetic data generated from nonlinear dynamical systems, but their potential for

the analysis of ISI sequences remains largely unexplored. A particularly useful tool is known as *symbolic analysis* [18]. In this approach, by defining an appropriated symbolic rule, a time-series is transformed into a sequence of symbols and its information content is described by a set of discrete probabilities, defined in terms of the frequencies of occurrence of the different symbols. Which symbolic rule is appropriated to quantify the information content of a time-series and to capture relevant properties (such as the presence of more expressed or less expressed symbols) depends on the specific system, as well as on the length and characteristics of the data. Different symbolic rules might capture different properties of the dynamics, providing complementary information [18].

A popular symbolic technique, known as *ordinal analysis* [19], has been proven very useful for investigating biomedical signals and other complex signals. It has been used for classifying behaviors, for detecting dynamical changes, for estimating model parameters, etc. [20–28]. Ordinal analysis uses symbols known as *ordinal patterns* of length L , which are defined in terms of the *relative order relations* of L data values. Because each symbol is determined by L values, temporal information is incorporated in the symbolic sequence. In contrast, when the encoding rule assigns a symbol to each individual data point, the resulting symbolic sequence can be regarded a coarse-grained description of the time series. One can then expect that ordinal analysis will provide additional, complementary information to that gained by SCCs. This is because SCCs performs a comparison of two ISI values with a global magnitude (the mean ISI, $\langle I \rangle$), while in contrast, ordinal analysis performs a relative comparison of each data-point with the $L - 1$ previous data-points. In addition, one can expect that ordinal analysis provides complementary information with respect to that gained from the statistical analysis of

the ISI sequence, because it keeps information about the presence of temporal ordering in the sequence of ISI values, while the ISI distribution does not (shuffle surrogate data has the same ISI distribution as the original data). On the other hand, because ordinal analysis neglects the actual ISI values (i.e., the precise duration of the interspike intervals), one can expect that SCCs and the ISI distribution will provide “amplitude” information that can not be obtained with ordinal analysis.

Here our goal is to analyze order relations in ISI sequences generated by a single neuron driven by *weak* periodic and stochastic inputs. We perform extensive simulations of the FitzHugh-Nagumo (FHN) model (a classical example of an excitable nonlinear system), driven by Gaussian white noise and a subthreshold sinusoidal input: without noise there are no spikes (but only subthreshold oscillations). The simulated ISI sequences are thus generated by the combined effects of noise and periodic forcing. Temporal correlations in the ISI sequence are detected and quantified by the probabilities of the ordinal patterns (OPs).

We demonstrate that these probabilities capture relevant properties of the ISI sequence: we find the presence of preferred patterns which are tuned by i) the period of the input signal and ii) the strength of the noise. We also show that some probabilities display the resonance-like feature of being enhanced for particular, signal-dependent noise levels. In addition, for certain parameters we find that the OP probabilities are organized in hierarchical structure, with clusters of two patterns having very similar probabilities. We conclude with a discussion of the relation between the OP probabilities, the mean ISI, and the SCCs.

MODEL

The FHN equations are [1]:

$$\epsilon \frac{dx}{dt} = x - \frac{x^3}{3} - y, \quad (2)$$

$$\frac{dy}{dt} = x + a + a_o \cos(2\pi t/T) + D\xi(t), \quad (3)$$

where x is the fast variable and y is the slow one, $\epsilon \ll 1$ and a is a control parameter such that, when $|a| > 1$ there is a stable fixed point, and when $|a| < 1$, there is a stable limit cycle; $\xi(t)$ is a white Gaussian noise of zero mean and unit variance and D is the noise strength; a_o and T are the amplitude and the period of the input signal.

The FHN model was simulated with parameters as in [1]: $a = 1.05$ and $\epsilon = 0.01$; a_o and T were varied such that the input signal is kept subthreshold (without noise there are no spikes). The model equations are integrated with random initial conditions and a second-order Runge-Kutta method, with integration step 0.005.

Figure 1 displays typical spike sequences, where the spike times, t_i , are detected by using a threshold. Then, the ISI sequence is defined as $\{I_i\}$, with $I_i = t_i - t_{i-1}$. For each set of parameters, time-series with more than 100,000 ISIs were generated (the first 100 ISIs were neglected to let transients die away).

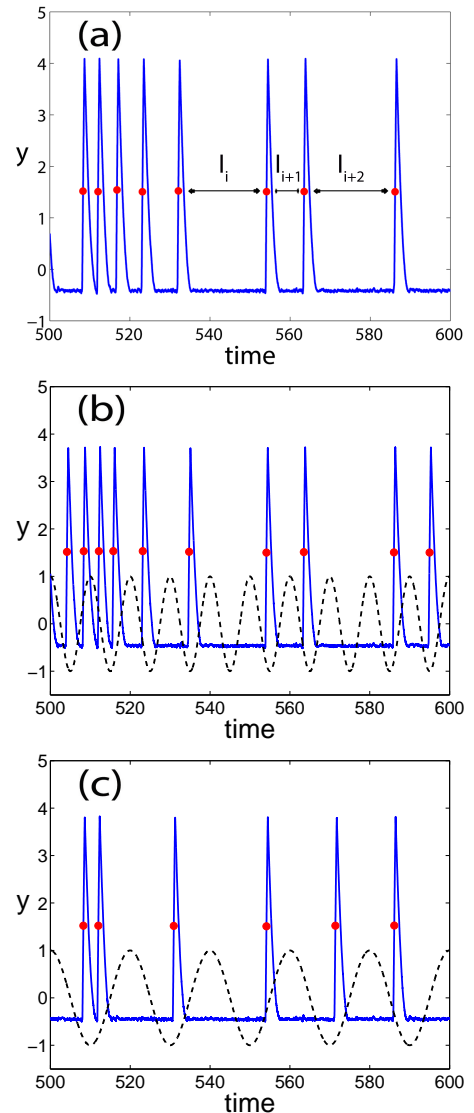


FIG. 1. (Color online) Time-series generated from the FHN model with parameters $a = 1.05$, $\epsilon = 0.01$, and $D = 0.015$. In (a) $a_o = 0$, while in (b) and (c) $a_o = 0.02$, $T = 10$ and $T = 20$ respectively. The spike times are detected with the threshold $y = 1.5$. In panels (b) and (c) the dashed line indicates the value of $\cos(2\pi t/T)$.

METHODS

As discussed in the Introduction, the OPs are defined by the relative ordering of L ISI values. Neglecting equality, for $L = 2$, $I_i < I_{i+1}$ gives pattern ‘01’ and $I_i > I_{i+1}$

gives ‘10’; for $L = 3$ the $L! = 6$ possible order relations are indicated in the inset of Fig. 2: $I_i < I_{i+1} < I_{i+2}$ gives pattern ‘012’; $I_{i+1} < I_i < I_{i+2}$ gives pattern ‘102’, etc. If $I_i = I_{i+1}$, a small random value is added before computing the ordinal pattern. Longer order relations can be analyzed by either using lags (considering non-consecutive values, $I_i, I_{i+\tau}$ and $I_{i+2\tau}$) or by using longer patterns (for $L = 4$ there are $4! = 24$ possible order relations, etc.). In this work we analyze consecutive ISIs ($\tau = 1$) and mainly focus on OPs of length $L = 3$, but we also analyze longer correlations with $L = 4$ and $L = 5$ OPs.

If the $L!$ patterns are equally probable, one can conclude that there are no preferred order relations among L consecutive ISI values; in contrast, a non uniform distribution of OP probabilities reveals the presence of preferred and/or infrequent order relations. The interval of probability values which is consistent with the uniform distribution is computed with a binomial test: if the OP probabilities are within the interval $[p-3\sigma, p+3\sigma]$, where $p = 1/L!$, $\sigma = \sqrt{p(1-p)/M}$, and M is the number of OPs, then, the probabilities are consistent with the uniform distribution with 95 % confidence level.

The set of ordinal probabilities, p_i with $i \in [1 \dots L!]$, has associated an entropy, known as *permutation entropy* [19, 27, 28], which is defined as $H = S/S_{max}$, with $S = -\sum p_i \log p_i$ and $S_{max} = \log L!$. The permutation entropy provides a complexity measure for time-series and even very small deviations from $H = 1$ can be used for detecting signatures of underlying determinism, for identifying dynamical changes and characteristic time-scales, etc. [21, 24–26, 29].

RESULTS

Let us first analyze the ISI sequence generated by the stochastic input only ($a_o = 0$). Figure 2(a) displays the probabilities of the six OPs as a function of the noise strength, and the grey region indicates the probability region consistent with the uniform distribution. We can observe that, within the range of noise strength considered, the six probabilities are in the grey region, and thus, they are consistent with equally probable patterns, i.e., no order relations are detected in the ISI sequence. This is interpreted as due to the fact that the spikes are induced by a fully random process (Gaussian white noise).

Next, we add the weak periodic input, and again plot the OP probabilities vs the noise strength [in Fig. 2(b), $T = 10$; in Fig. 2(c), $T = 20$]. We observe a resonance-like phenomenon, in which the probabilities of some patterns lie outside the grey region for certain noise strengths. For example, in Fig. 2(b), we note that for $D \sim 0.03$, ‘V’ and ‘Λ’ are the preferred patterns; in Fig. 2(c), with weak noise ‘V’ and ‘Λ’ are preferred, but with higher noise, ‘012’ and ‘210’ are preferred.

The effect of the periodic signal gradually increases with its amplitude. This is shown in Fig. 3 that displays the OP probabilities vs. a_o , keeping fixed the period of the signal and the strength of the noise. We consider weak noise [Fig. 3(a)] and stronger noise [Fig. 3(b)], which induce different ISI order relations [as indicated with arrows in Fig. 2(c)]. We observe that, in both cases, as a_o increases, the OP probabilities gradually leave the grey region, revealing that order relations gradually emerge in the ISI sequence. We note that, within the range of values considered here (the input is sub-threshold), a_o does not change the preferred OPs.

In order to investigate the role of the period of the input signal, in Fig. 4 we display the OP probabilities vs. T . We consider weak and stronger noise (the same levels as in Fig. 3). We note that when the input signal is fast, the OP probabilities are inside the grey region, but for slower input, they lie outside. We also note that the preferred patterns depend on both, T and D , and there is a resonant-like effect in the form of enhanced probability of particular OPs for specific values of T and D . For example, for $D = 0.035$ [Fig. 4(b)] patterns ‘012’ and ‘210’ are preferred for $T \sim 6$, but they are unlikely to occur for $T \sim 10$.

To explore the length of temporal ordering, we show in Fig. 5(a), for the same parameters as Fig. 4(b), the probabilities of OPs of length $L = 2$. We observe that they are in the grey area, which indicates that there is no temporal order in the ISI sequence. However, the probabilities of $L = 3$ OPs revealed the presence of patterns with favored occurrence, as it was shown in Fig. 4(b). Therefore, we conclude that, in order to uncover temporal ordering, the ISI sequence has to be analyzed with OPs of appropriate length: if the length of the OP is too short, no temporal ordering is detected (as shown here, with $L = 2$ OP the probabilities are within the grey area consistent with equi-probable OPs), while if the length of the OP is too long, as will be shown below, the large number of OPs will require very long time-series in order to compute the OP probabilities with robust statistics.

To explore the effect of longer OPs, it is unpractical to display the probabilities of 24 $L = 4$ OPs or 120 $L = 5$ OPs. Therefore, in Fig. 5(b) we plot the permutation entropy, H , computed with patterns of length $L=3, 4$, and 5 vs. the period of the input signal. The value of H very close to 1 indicates that the time-series is highly stochastic. This is expected because the modulation is subthreshold and the spikes are noise-induced. However, a small variation of the permutation entropy is a signature of a transition as T increases: for $T < 5$, $H \sim 1$, while for longer T , H tends to decrease, but non-monotonically, i.e., there are values of T for which H is minimum, indicating the existence of more probable patterns and thus, temporal ordering in the ISI sequence. We also note that, while for $T < 5$ $H \sim 1$ for $L = 3 - 5$, for $T > 5$, the permutation entropy decreases with L ,

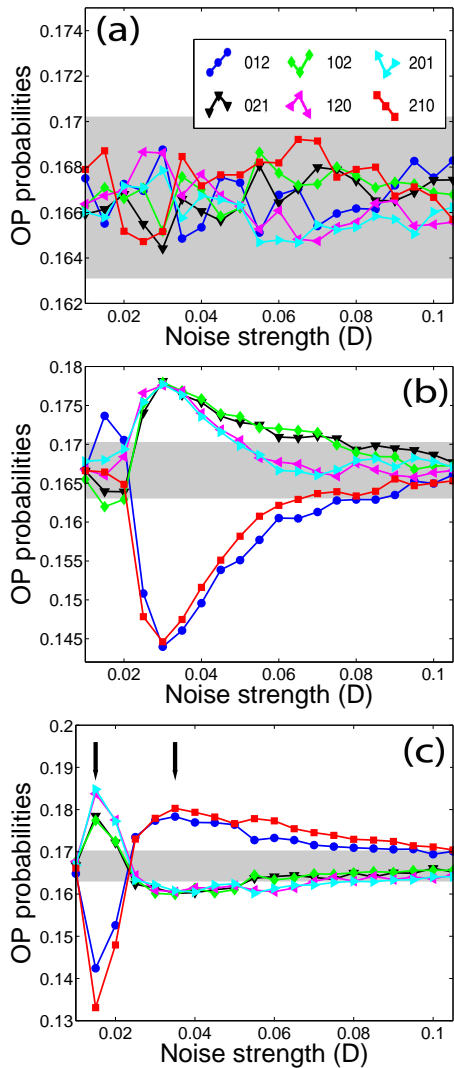


FIG. 2. (Color online) Probabilities of the six ordinal patterns (OPs) that are defined by the relative length of three consecutive inter-spike-intervals (ISIs) vs. the noise strength. The OPs are schematically shown in the inset. The parameters are (a) $a_o=0$, (b) $a_o=0.02$, $T=10$, (c) $a_o=0.02$, $T=20$; other parameters are as indicated in the text. In panel (c), the arrows indicate the noise levels used in Figs. 3 and 4.

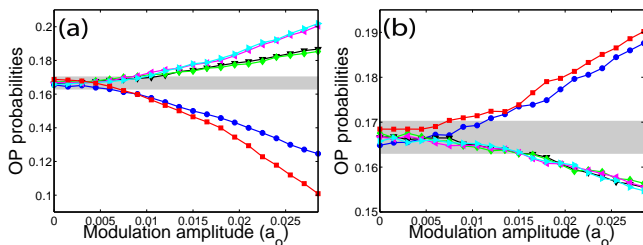


FIG. 3. (Color online) OP probabilities vs. the amplitude of the input signal. The parameters are $T=20$, (a) $D=0.015$ and (b) $D=0.035$, other parameters as in Fig. 1.

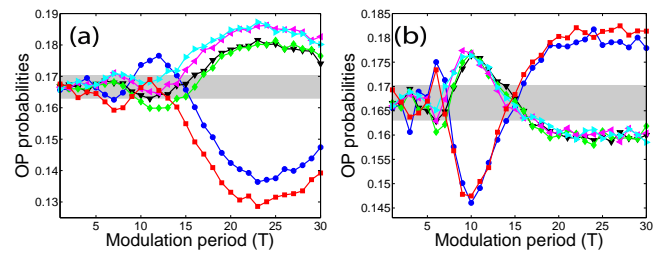


FIG. 4. (Color online) OP probabilities vs. the period of the input signal. The parameters are $a_o=0.02$, (a) $D=0.015$ and (b) $D=0.035$, other parameters as in Fig. 1.

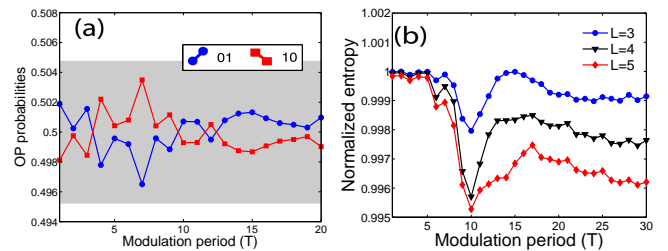


FIG. 5. (Color online) (a) Probabilities of patterns ‘01’ and ‘10’ vs. the period of the input signal. (b) Permutation entropy vs. T for OPs of length $L=3, 4$, and 5 . In panels (a) and in (b) the parameters are as in Fig. 4(b).

indicating the longer range of temporal ordering.

The influence of the length of the time series, M , is shown in Fig. 6 that displays the OP probabilities vs. M . We see that, with a periodic input signal [panels 6(a) and 6(b)], the OP probabilities are outside the grey region, if M is large enough. Moreover, in panel 6(b), “clusters” of OPs with similar probabilities are seen, only if $M \gg 10^3$ (similar clustering was reported in [30]). In contrast, without periodic input [panel 6(c)] the probabilities are inside the grey region and no clustering is seen, even for large M .

Interestingly, the behavior of the OP probabilities seen in Fig. 3(a) resembles that found experimentally in a modulated semiconductor laser that emits feedback-induced optical spikes [30]. As shown in Fig. 4(a) in [30], when the modulation amplitude increases there is a transition to a dynamical state in which some OP probabilities are outside the grey region, and, remarkable, the OP probabilities are organized in the same “clusters”, and with the same hierarchy (the same ordering of the OP probabilities) as observed in Fig. 3(a) here. This qualitative similarity can be due to a generic behavior of excitable systems, that can be described by circle maps [31]. As shown in [30], a modified circle map qualitatively explains the behavior of the OP probabilities computed from the laser data, and it has been shown to also explain serial correlations in empirical ISI data [17]. This suggests that similar behavior can be observed in other excitable systems.

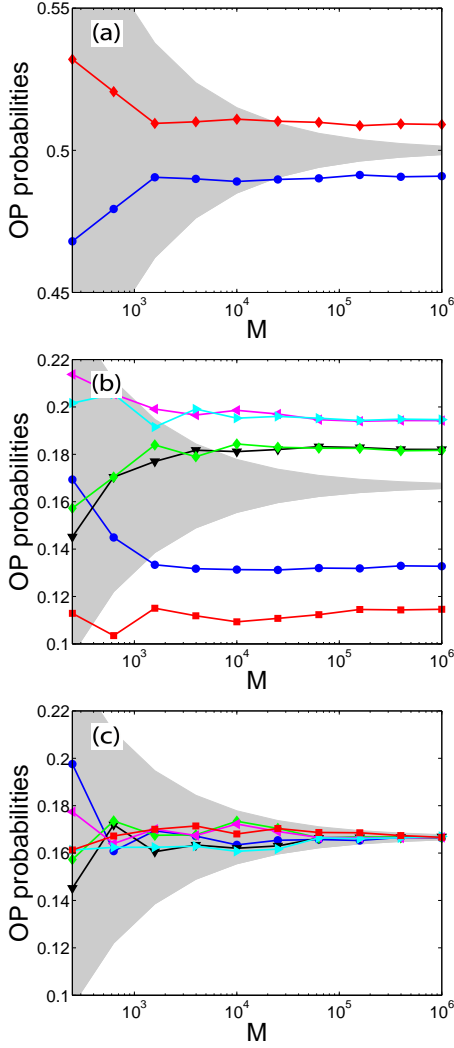


FIG. 6. (Color online) (a) Probabilities of patterns ‘01’ and ‘10’ vs. the number, M , of inter-spike intervals in logarithmic scale. (b) Probabilities of the 6 $L = 3$ OPs vs M . For both, (a) and (b), the parameters are $a_o = 0.025$, $D = 0.015$ and $T = 20$. (c) Same as panel (b) but with $a_o = 0$.

COMPARISON WITH MEAN-ISI AND CORRELATION ANALYSIS

Since both, the noise strength, D , and the period of the input signal, T , modify the neuron’s spike rate, one could expect that the underlying reason for the variation of the OP probabilities with D and T is related to the spike rate variation. One could also wonder if these changes are also captured by correlation analysis.

To investigate if there is a close relation between the values of the OP probabilities and the serial correlation coefficients, C_1 and C_2 , and the mean ISI, $\langle I \rangle$ (the inverse of the spike rate), Figs. 7-9 display, for the same parameters as Figs. 2-4, C_1 and C_2 (center column) and the mean ISI (right column). For easy comparison, the

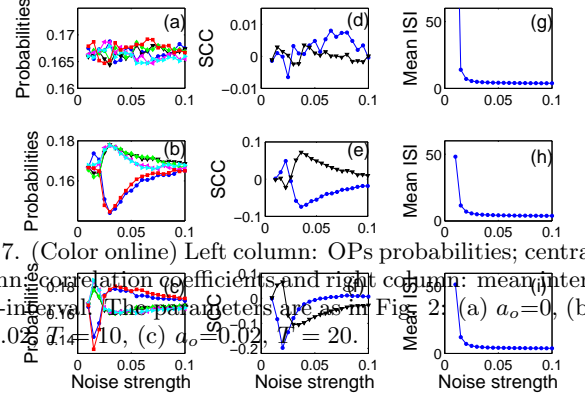


FIG. 7. (Color online) Left column: OPs probabilities; central column: correlation coefficients, and right column: mean inter-spike-interval. The parameters are as in Fig. 2: (a) $a_o=0$, (b) $a_o=0.025$, (c) $a_o=0.02$, $T=20$.

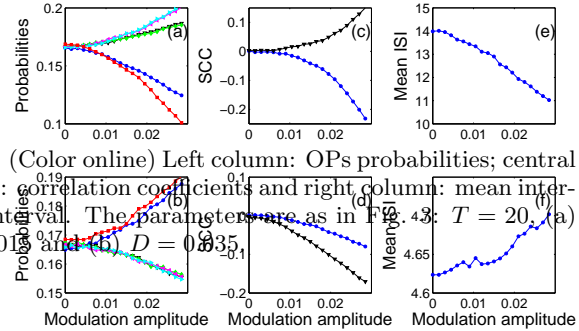


FIG. 8. (Color online) Left column: OPs probabilities; central column: correlation coefficients and right column: mean inter-spike-interval. The parameters are as in Fig. 4: (a) $T = 20$, (b) $T = 20$, (c) $T = 20$, (d) $T = 20$.

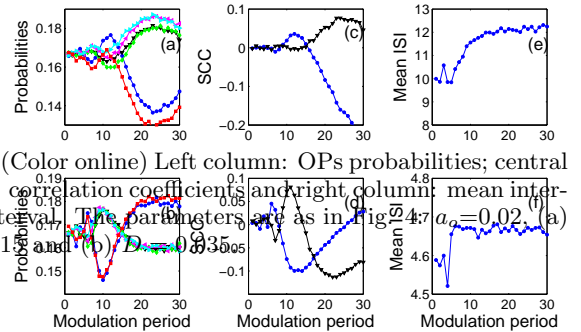


FIG. 9. (Color online) Left column: OPs probabilities; central column: correlation coefficients and right column: mean inter-spike-interval. The parameters are as in Fig. 4: (a) $a_o=0.02$, (b) $a_o=0.02$, (c) $a_o=0.02$, (d) $a_o=0.02$.

OP probabilities are also shown in the left column.

First, we note that the variation of $\langle I \rangle$ with D and T is not correlated to that of the OP probabilities: in particular, we see no similar trend. Second, we note that C_1 and C_2 display smooth variations, similar to those of the OP probabilities. As expected, when $C_1 < 0$ and $C_2 > 0$ the most expressed OPs are Vs and As ('021', '120', '201', '102').

In addition, under particular conditions "equivalent situations" can be identified. For example, in Fig. 9 first row, for $T = 20$ and $D = 0.015$, $\langle I \rangle = 12 \sim T/2$. In this case, patterns '012' and '210' are the less expressed. Comparing with the second row (for $D = 0.035$), for $T = 10$, $\langle I \rangle = 5 \sim T/2$, and also patterns '012' and '210' are the less expressed. The two situations are "equivalent" because in both cases $\langle I \rangle \sim T/2$, and when $T = 20$ and $D = 0.015$ (Fig. 9, first row): $C_1 \sim -0.08$ and $C_2 \sim +0.05$, while when $T = 10$ and $D = 0.035$ (Fig. 9, second row), $C_1 \sim -0.08$ and $C_2 \sim +0.05$.

However, in general, no clear relations can be inferred from these plots. In order to search for such relation, in Fig. 10 we have collapsed all data sets in scatter plots, which display the OP probabilities vs. C_1 and C_2 . For clarity the OP probabilities are separated in three groups: the trend patterns ('012' and '210' in the left column of Fig. 10), and the two clusters of patterns that have similar probabilities ('021' and '102' in the center column and '120' and '201' in the right column). In the scatter plots no clear relations between C_1 and C_2 and the OP probabilities are seen, but there is a well-defined trend with C_2 (however, the relation is not one-to-one).

To further explore the relation between the OP probabilities and the serial correlation coefficients we have re-done the scatter plots, now plotting the pattern probability in color code vs. C_1 and C_2 . Figures 11(a) and 11(b) display the probability of the trend pattern '012' and of the 'V' pattern '102', respectively, again collapsing all data sets shown in Figs. 7-9. Here again we see a clear trend with C_2 but no trend with C_1 . We note that the trend pattern '012' (the 'V' pattern '102') is less probable (is more probable) if $C_1 < 0$ and $C_2 > 0$. We again note that the relation is not one-to-one and similar values of C_1 and C_2 might correspond to different values of the ordinal probabilities, thus, the ordinal probabilities cannot be predicted from knowledge of ISI statistics; however, the trends seen in these plots allow predicting that if $C_1 < 0$ and $C_2 > 0$, pattern '012' (pattern '102') will be less (more) expressed than expected if the six patterns are equally probable.

We conclude this section by summarizing the information gained with ordinal analysis, which could not be inferred from correlation analysis:

i) For a wide range of parameters, in the ISI sequences there are OPs which have almost equal probabilities: '021', '102' and '201', '120'.

ii) For a wide range of parameters, there is a well-

defined hierarchy in the probabilities of the various OPs. For example, in Fig. 7(b), for $D > 0.04$,

$$P(102) = P(021) > P(120) = P(201) > P(210) > P(012),$$

while in Fig. 9(a), for $T > 15$,

$$P(120) = P(201) > P(102) = P(021) > P(012) > P(210).$$

iii) The ordinal probabilities allow computing the permutation entropy, shown in Fig. 5(b), that displays a sharp transition at $T = 10$. Such transition is not seen in $\langle I \rangle$, C_1 or C_2 , which vary smoothly with the modulation period (as shown in Fig. 9).

These observations provide a complementary approach for a qualitative comparison of empirical and synthetic ISI sequences, and can also be useful for distinguishing/classifying different types of ISI sequences.

CONCLUSIONS

To summarize, we have studied the emergence of relative temporal order in spike sequences induced by the interplay of a stochastic input and a subthreshold periodic input. By using symbolic analysis we uncovered preferred ordinal patterns, which are tuned by the period of the input signal and by the strength of the noise. We have also shown that the probabilities of specific patterns are maximum or minimum for particular values of the period of the input and the strength of the noise. Our findings could be useful for contrasting empirical and synthetic ISI sequences, for validating neuron models or estimating their parameters. Moreover, our results could motivate new experiments on single sensory neurons, to further understand the mechanisms by which they encode information about weak stimuli in noisy environments.

This work has been supported in part by the Spanish MINECO (FIS2015-66503-C3-2-P). C. M. also acknowledges partial support from ICREA ACADEMIA, Generalitat de Catalunya.

* aparicioreinoso@gmail.com

† carme.torrent@upc.edu

‡ cristina.masoller@upc.edu

- [1] A. S. Pikovsky and J. Kurths, *Phys. Rev. Lett.* **78**, 775 (1997).
- [2] A. Longtin, *J. Stat. Phys.* **70**, 309 (1993).
- [3] C. Heneghan, C. C. Chow, J. J. Collins, T. T. Imhoff, S. B. Lowen, and M. C. Teich, *Phys. Rev. E* **54**, R2228 (1996).
- [4] L. Gammaitoni, P. Hnggi, P. Jung, and F. Marchesoni, *Rev. Mod. Phys.* **70**, 223 (1998).
- [5] M. D. McDonnell, N. Iannella, M. S. To, H. C. Tuckwell, J. Jost, B. S. Gutkin, and L. M. Ward, *Network: Computation in Neural Systems* **0**, 1-37 (2015).

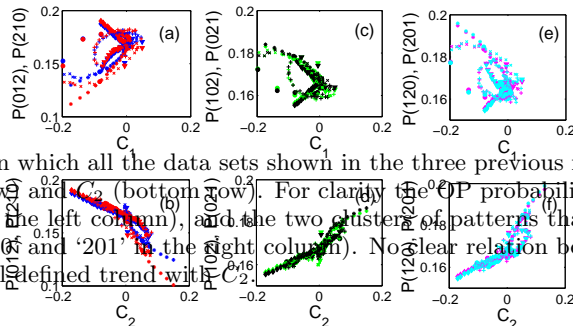


FIG. 10. (Color online) Scatter plots in which all the data sets shown in the three previous figures are collapsed. Here the OP probabilities are plotted vs C_1 (top row) and C_2 (bottom row). For clarity the OP probabilities are separated in three groups: the trend patterns ('012' and '210', in the left column), and the two clusters of patterns that have similar probabilities ('021' and '102' in the center column and '120' and '201' in the right column). No clear relation between C_1 , C_2 , and the six ordinal probabilities is seen, but there is a well-defined trend with C_2 .

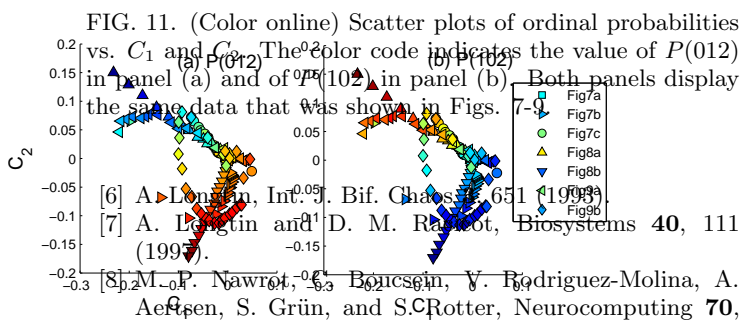


FIG. 11. (Color online) Scatter plots of ordinal probabilities vs. C_1 and C_2 . The color code indicates the value of $P(012)$ in panel (a) and of $P(102)$ in panel (b). Both panels display the same data that was shown in Figs. 7-9.

- [6] A. Longtin, *Int. J. Bif. Chaos* **6**, 651 (1996).
- [7] A. Longtin and D. M. Rabalet, *Biosystems* **40**, 111 (1997).
- [8] M. P. Nawrot, V. Boucsein, V. Rodriguez-Molina, A. Aertsen, S. Grün, and S. Rotter, *Neurocomputing* **70**, 1717 (2007).
- [9] L. Shau, U. Schwab, and B. Lindner, *J. Comput. Neurosci.* **38**, 589 (2015).
- [10] M. J. Chacron, A. Longtin, and L. Maler, *Journal of Neuroscience* **21**(14), 5328 (2001).
- [11] M. J. Chacron, B. Lindner, and A. Longtin, *Phys. Rev. Lett.* **92**, 080601 (2004).
- [12] S. P. Strong, R. Koberle, R. R. de Ruyter van Steveninck, and W. Bialek, *Phys. Rev. Lett.* **80**, 197 (1998).
- [13] F. Farkhooi, M. F. Strube-Bloss, and M. P. Nawrot, *Phys. Rev. E* **79**, 021905 (2009).
- [14] A. Longtin and D. R. Chialvo, *Phys. Rev. Lett.* **18**, 4012

- (1998).
- [15] A. B. Neiman and D. F. Russell, *Phys. Rev. Lett.* **86**, 3443 (2001).
- [16] J. W. Middleton et al. *Phys. Rev. E* **68**, 021920 (2003).
- [17] A. B. Neiman, and D. F. Russell, *Phys. Rev. E* **71**, 061915 (2005).
- [18] C. S. Daw, C. E. A. Finney and E. R. Tracy, *Rev. Sci. Instrum.* **74**, 915 (2003).
- [19] C. Bandt and B. Pompe, *Phys. Rev. Lett.* **88**, 174102 (2002).
- [20] C. Bandt *Ecological Modelling* **182**, 229 (2005).
- [21] O. A. Rosso, H. A. Larrondo, M. T. Martin, A. Plastino, and M. A. Fuentes, *Phys. Rev. Lett.* **99**, 154102 (2007).
- [22] U. Parlitz, S. Berg, S. Luther, A. Schirdewan, J. Kurths, and N. Wessel, *Comp. Biol. Med.* **42**, 319 (2012).
- [23] G. Graff, B. Graff, A. Kaczkowska, D. Makowiec, J. M. Amigó, J. Piskorski, K. Narkiewicz, and P. Guzik, *Eur. Phys. J. Spec. Top.* **222**, 2 (2013).
- [24] Y. Cao, W. W. Tung, J. B. Gao, V. A. Protopopescu, and L. M. Hively, *Phys. Rev. E* **70**, 046217 (2004).
- [25] C. Masoller, Y. Hong, S. Ayad, F. Gustave, S. Barland, A. J. Pons, S. Gomez, and A. Arenas, *New J. of Phys.* **17**, 023068 (2015).
- [26] A. Aragoneses, L. Carpi, N. Tarasov, D. V. Churkin, M. C. Torrent, C. Masoller, and S. K. Turitsyn, *Phys. Rev. Lett.* **116**, 033902 (2016).
- [27] M. Zanin, L. Zunino, O. A. Rosso, and D. Papo, *Entropy* **14**, 1553 (2012).
- [28] J. M. Amigó, K. Keller, and J. Kurths, *Eur. Phys. J. Spec. Top.* **222**, 2 (2013).
- [29] M. C. Soriano, L. Zunino, O. A. Rosso, I. Fischer, and C. R. Mirasso, *IEEE J. Quantum Electron.* **47**, 252 (2011).
- [30] A. Aragoneses, S. Perrone, T. Sorrentino, M. C. Torrent, and C. Masoller, *Sci. Rep.* **4**, 4696 (2014).
- [31] M. Feingold, D. L. Gonzalez, O. Piro, and H. Viturro, *Phys. Rev. A* **37**, 4060 (1988).